Phonon-assisted tunneling in persistent-photocurrent decay

L. X. He
Department of Physics, University of Oregon, Eugene, Oregon 97403

K. P. Martin* and R. J. Higgins
School of Electrical Engineering and Microelectronics Research Center, Georgia Institute of Technology, Atlanta, Georgia 30332

(Received 27 June 1988)

While in bulk $Al_xGa_{1-x}As$ there is some agreement that persistent photoconductivity (PPC) is related to the photoionization of deep levels that have a recombination barrier, a diverse collection of models has been proposed to explain the interplay between macroscopic (band bending and tunneling) and microscopic (deep levels) contributions to PPC and related phenomena in $GaAs/Al_xGa_{1-x}As$ heterostructures. One of these related effects is transient photoconductivity (TPC) whereby the PPC-enhanced carrier density (or conductivity) undergoes a long-term decay. In this work a model based on phonon-assisted tunneling through a realistic barrier is developed for TPC, and predictions for the apparent capture energies and lifetime prefactors are presented. The model self-consistently accounts for the changes in the conduction-band profile and tunneling barrier due to the transfer of charge during this process. By using the derivative of conductivity or carrier number density with respect to the logarithm of time during decay, e.g., $dN/d(\ln t)$, phonon-assisted tunneling may be identified from other PPC-associated decay mechanisms in $GaAs/Al_xGa_{1-x}As$ heterostructures. This method of analysis is applied to experimental data showing TPC decay of carrier density and conductivity. The *DX*-center capture energies obtained from phonon-assisted-tunneling data in this work agree with results from other direct-capture studies.

I. INTRODUCTION

Persistent photoconductivity (PPC) is well known for many semiconductor materials and configurations.[1] It is important to understand PPC and related effects in modulation-doped materials and high-electron-mobility transistors (HEMT's) formed from $GaAs/Al_xGa_{1-x}As$ heterostructures at $T < 180$ K where HEMT's display optimal electronic properties. In bulk materials, PPC is generally understood to occur by the photoionization of deep levels that have a recombination barrier. However in $GaAs/Al_xGa_{1-x}As$-based heterostructures and devices a variety of models have been proposed to explain the interplay between macroscopic[2,3] (band bending) and microscopic[4,5] (deep levels) mechanisms for PPC. Microscopic-barrier models are based on postulated atomic-scale barriers that suppress recombination of free carriers. The carriers are photoexcited from the impurity center, a deep-donor complex (predominantly identified as the *DX* center in Si-doped $Al_xGa_{1-x}As$) with optical thresholds smaller than the band gap of the material. The origin of these deep donors has not been fully clarified but they are usually described as impurity-atom-plus-defect complexes with large lattice relaxations. The earliest model[5] for *DX* centers in doped $Al_xGa_{1-x}As$ is a donor-vacancy (As) complex, which requires an As vacancy number density as high as 1×10^{18} cm^{-3}. Recently a donor-self-generated-vacancy model has been proposed to avoid this high density of As vacancies.[6]

The decay of PPC-enhanced carrier density and mobility has been experimentally observed by a number of workers.[3,7–9] Transient photoconductivity (TPC) occurs on time scales as long as 10^5 sec and at temperatures as low as 4.2 K. Tunneling[3] provides an important mechanism for electrons to move between the GaAs and $Al_xGa_{1-x}As$ layers despite the macroscopic barrier presented by the conduction band (Fig. 1). In this work a TPC-decay model based on tunneling between the two-dimensional electron gas (2D EG) and states in the $Al_xGa_{1-x}As$-layer conduction band is presented. The transfer of electrons is accompanied by the corresponding self-consistent changes in the conduction-band profile and tunneling barrier. The model incorporates a realistic representation of the heterojunction barrier and band discontinuity into a Wentzel-Kramers-Brillouin (WKB) calculation of the tunneling probability. The lifetime of tunneling-assisted capture is determined by the tunneling probability and the capture cross section of the traps. When kT is much smaller than the height of the tunneling barrier, a WKB calculation shows that the tunneling probability only depends on the tunneling-barrier shape. At high enough temperatures, phonon-assisted tunneling becomes important.

The result of this model is a prediction of apparent capture energies and lifetime prefactors of the decay processes. Experimental measurements of persistent-photocurrent decay in different gated and ungated heterostructure material are shown to agree quite well with

these predictions. The data is analyzed by a method using a derivative of number density (or conductivity) with respect to the logarithm of time. The decay features brought out by this analysis are identified with different decay processes.

II. THEORETICAL MODEL

When the 2D EG is confined in the potential well at the $Al_xGa_{1-x}As/GaAs$ interface (Fig. 1), the z component of the electron wave function is separated from the xy component, and the z-direction energy is quantized with a ground-state energy E_0 above the conduction band. TPC tunneling is in the z direction and starts from the $Al_xGa_{1-x}As/GaAs$ interface with a carrier energy of E_0 plus the 2D EG thermal energy E_{th}. The effective tunneling barrier is the conduction-band profile above E_0+E_{th} (Fig. 1).

As the tunneling electrons first move into the conduction band in the $Al_xGa_{1-x}As$ layer, the tunneling barrier is different for the remaining 2D electrons [short-dashed curve, Fig. 1(a)] because of the decreased 2D EG density (N_{2D}) and the decrease in the depletion width W_d. This

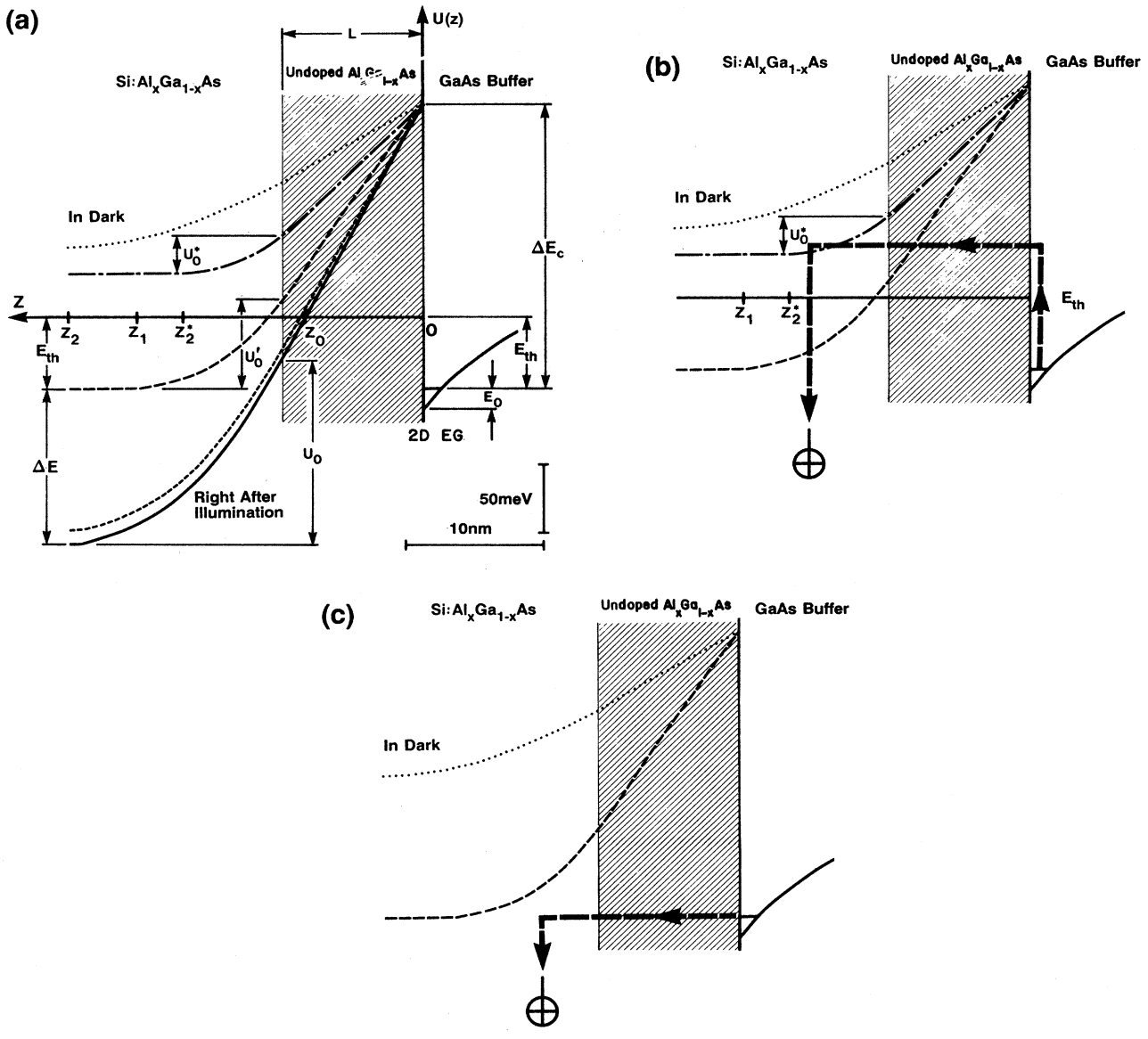

FIG. 1. Tunneling mechanisms and typical conduction-band tunneling barriers $U(z)$ (see the Appendix) for a $GaAs/Al_{0.3}Ga_{0.7}As$ heterostructure. The dotted curve is the barrier at 77 K in-dark (100 meV above E_0) (Ref. 8). The solid curve (a) is the barrier right after illumination ($W_d=15$ nm, $\Delta E=120$ meV). The long-dashed curve ($W_d=11$ nm, $\Delta E=0$) is at the end of type-A tunneling. After further decay, the barrier shown as a dot-dashed curve ($W_d=7$ nm, the conduction band is 80 meV above E_0) allows only type-B tunneling (b) and electron-impurity tunneling (c) to occur. The scales of the drawings are from the actual conditions of doping ($N_d=1\times10^{18}$ cm^{-3}) and illumination used.

larger tunneling barrier reduces the tunneling probability, and consequently the next carriers through have longer tunneling lifetimes. This process (designated as type-A tunneling) is completed when $W_d=(z_1-L)$ and the lowest value of the conduction band in the $Al_xGa_{1-x}As$ layer, E_{CB} is in equilibrium with the 2D EG. At this point the conduction-band bending appears as the long-dashed curve in Fig. 1(a).

In other circumstances, when E_{CB} moves above E_0 for further photodecay [dot-dashed curve in Fig. 1(b)] the 2D electrons will not be able to tunnel and stay in the $Al_xGa_{1-x}As$ layer unless there are unoccupied traps below E_0. This will be referred to as type-B tunneling-assisted decay.

Consider a heterostructure with a relatively small band discontinuity at a high temperature (e.g., $\Delta E_c=0.23$ eV, and $kT=0.01$ eV at 100 K) and a doping density $N_d=10^{18}$ cm^{-3}. The pure-tunneling probability (10^{-6}–10^{-10}) estimated from the WKB integral of the conduction-band profile is comparable with the thermal-activation probability $\exp(-\Delta E_c/kT)$. In this case TPC can be described as a phonon-assisted process with a tunneling probability:

$$P=A\int \exp\left[-E_{\rm th}/kT - \int (4\pi/h)[2m^*U(z)]^{1/2}dz\right]dE_{\rm th}\ , \qquad (1)$$

where m^* is the effective mass of an electron in the $Al_xGa_{1-x}As$ layer, and $E_{\rm th}$ is the thermal energy of the tunneling electron. $U(z)$ is the tunneling barrier measured from $E_0+E_{\rm th}$. The WKB integral ($\int (4\pi/h)[2m^*U(z)]^{1/2}dz$) is evaluated from $z=0$ to z_0, where z_0 is the point where the $Al_xGa_{1-x}As$ conduction band is even with $E_0+E_{\rm th}$ [Fig. 1(a)]. When the WKB integral is bigger than $E_{\rm th}/kT$, the normalization factor A is only weakly temperature dependent. Detailed expressions for $U(z)$ and z_0 are shown in the Appendix for a given $E_{\rm th}$, ΔE_c, L, and ionized donor density N_i.

Figure 2 shows the temperature-dependent tunneling lifetime τ numerically determined from Eq. (1) over a range of W_d. It is clear that at a fixed temperature, τ monotonically *increases* during TPC decay while W_d *decreases.* The lifetime can increase as much as four orders of magnitude for a factor of 2 change in W_d. It should also be noted that for type-A decay τ is weakly temperature dependent for $T<100$ K, but becomes strongly temperature dependent above 100 K because of phonon-assisted tunneling. An activation energy E_t can be determined from the slope of τ versus $1/T$ for a fixed W_d, and in the high-temperature limit E_t would approach ΔE_c.

Actually, N_i (following illumination) is a function of T because at high temperatures the deep-trap recombination rate can be comparable with the photoemission rate. Using the temperature dependence of N_i,[10] (for an Al fraction $x=0.3$) results in an apparent $E_t\sim 170$ meV at 160 K, but about 20 meV at 70 K, for $W_d=(z_1-L)$ and $N_d=1\times10^{18}$ cm^{-3}.

Although the difference in mobility between 2D electrons and carriers in the $Al_xGa_{1-x}As$ layer allows pure tunneling to be detected, the times (10^{-8}–10^{-4} sec) (Ref. 11) are too short to be observed in this experiment. When this process is completed, direct capture of electrons in the $Al_xGa_{1-x}As$ layer by nearby traps can be detected, generally with a longer, trap-dependent lifetime. In the case of shallow traps, τ is assumed to be weakly temperature dependent, and on the order of 10^{-3}–10^{-2} sec. However for deep traps such as DX centers, τ is strongly temperature dependent.

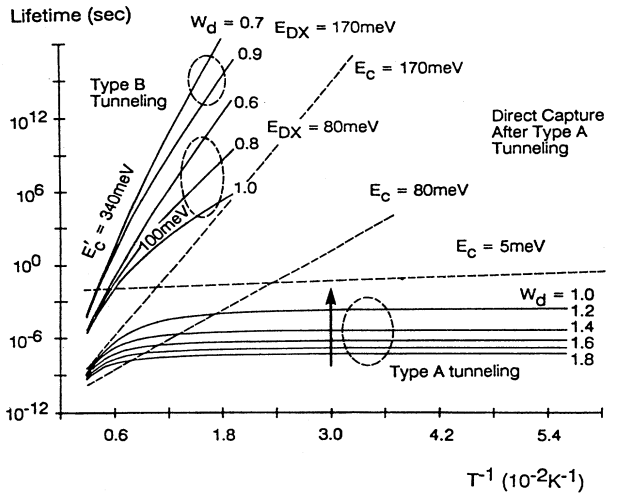

FIG. 2. The predicted TPC lifetimes. The arrow denotes the time evolution of type-A tunneling for fixed T [starting from $W_d=1.8(z_1-L)$ and ending at $W_d=1.0(z_1-L)$]. Also shown is type-B tunneling-assisted decay with DX-center capture energies of either 80 meV [decay from $W_d=1.0(z_1-L)$ to $W_d=0.6(z_1-L)$] or 170 meV [decay from $W_d=0.9(z_1-L)$ to $W_d=0.7(z_1-L)$]. For comparison, lifetimes from direct capture in the $Al_xGa_{1-x}As$ layer by shallow ($E_c=5$ meV) or deep traps ($E_c=80$ or 170 meV) after type A are represented as dashed lines.

The capture lifetime of a conduction-band electron in the $Al_xGa_{1-x}As$ layer trapped by a DX center is expressed as

$$\tau=\tau_0\exp(E_{DX}/kT)\ , \qquad (2)$$

where E_{DX} is the capture energy, and $\tau_0\sim10^{-11}$ sec.

So in the case of type-B tunneling the lifetime of a 2D electron captured by DX centers is expressed by

$$\tau=[\tau_0\exp(E_{DX}/kT)]P^{-1}\ . \qquad (3)$$

Here the tunneling probability is calculated from Eq. (1) and the Appendix, with the integral over $E_{\rm th}$ beginning from E_{CB} [dashed line, Fig. 1(b)].

Over a narrow temperature range, the phonon-assisted tunneling probability P may be expressed as $P=P_0\exp(-E_t/kT)$, and one has

$$\tau=\tau_0^*\exp[(E_{DX}+E_t)/kT] \qquad (4)$$

with $\tau_0^*=\tau_0P_0^{-1}$ and an apparent capture energy $E_c'=E_{DX}+E_t$. Notice that E_t and P are temperature

dependent. Considering that $P_0=1$ for phonon-assisted tunneling in the high-temperature limit, the value of τ_0^* should be the same as the case for direct capture by deep traps at high temperatures, i.e., $\tau_0^* \sim 10^{-11}$ sec. At lower temperatures ($T \sim 77$ K), $P_0 \ll 1$, and $\tau_0^* \gg \tau_0$.

The calculated results for type-B tunneling-assisted capture into deep traps are also plotted in Fig. 2 using DX-center capture energies $E_c=80$ and 170 meV. Note that E_c' taken from the slope of the curves in Fig. 6 is 100 meV at 77 K for $E_{DX}=80$ and 340 meV at 160 K for $E_{DX}=170$ meV.

For comparison direct capture in the $Al_xGa_{1-x}As$ layer by shallow or deep traps after type-A tunneling is plotted in Fig. 2 as dashed lines, with shallow-trap capture energies equal to 5 meV, and deep-trap capture energies chosen as 80 and 170 meV.

Another type of tunneling process that could contribute to TPC is electron-impurity tunneling[3] [Fig. 1(c)]. This mechanism suggests that 2D electrons tunnel into the $Al_xGa_{1-x}As$ depletion region and then are captured by deep traps. The trapping begins with donor traps nearest the 2D EG. While the initial 2D EG states and final trapped states have to be real, the intermediate states (e.g., in the forbidden gap) do not have to be real, but can be regarded as virtual states.[12] Though the detailed nature of the "virtual states" are not fully clarified, recapture dynamics of this tunneling would follow a decay curve with a much longer lifetime prefactor due to a small tunneling probability. For example, experiments at temperatures below 100 K have shown[3] that the lifetime prefactors are of the order of 1 sec, and the effective capture energy is estimated to be below 10 meV.

We now summarize the key results from Fig. 2 and make some predictions (excluding electron-impurity tunneling). For $T<50$ K, the observable capture within a time window of $10^{-3}-10^4$ sec is only shallow-donor related. For higher temperatures both shallow and deep traps can be involved.

Because the $Al_xGa_{1-x}As$-layer conduction band moves up with respect to E_0 during photodecay, tunneling-assisted capture can change from type-A to type-B tunneling. When all donors are photoionized [Fig. 1(a)] there is a large depletion width and low $Al_xGa_{1-x}As$ conduction-band minima so that type-A tunneling-assisted capture initially takes place. After a sufficiently long decay time, the $Al_xGa_{1-x}As$ conduction band is above E_0 but below the original in-dark conduction band [Fig. 1(b)], and then type-B tunneling-assisted capture takes place.

As an example, consider the case of $T=77$ K in Fig. 2. Direct capture by 80 meV deep centers and type-A tunneling occurs too quickly to be detected within an experimental time window of $10^{-3}-10^4$ sec of this work. Instead the first process to be observed is direct capture by shallow donors. Then, if the $Al_xGa_{1-x}As$-layer conduction band moves above E_0, type-B tunneling-assisted decay (with 80 meV deep traps) can be detected. E_c' will be about 100 meV due to the additional E_{th} at 77 K, and $\tau_0 \sim 10^{-5}$ sec (y intercept of the slope in Fig. 2), which is much longer than the DX-center capture prefactor of 10^{-11} sec. Alternatively, if the $Al_xGa_{1-x}As$ layer conduction band does not move above E_0, as in the case of a wide, doped layer with a large number of free electrons in it, direct capture to 170 meV deep traps dominates.

When the temperature is as high as 160 K, the first process to be seen within the same time window ($10^{-3}-10^4$ sec) is direct capture by shallow traps. The next process to appear is type-B tunneling-assisted capture by 170 meV deep traps. In this case, E_c' (about 340 meV) will be much large than the DX-center capture energy 170 meV, but the lifetime prefactor remains close to the value of 10^{-11} sec.

III. SAMPLES AND MEASUREMENTS

The molecular-beam-epitaxy- (MBE-) grown heterostructure samples in this work had the following layer sequence: Si-doped GaAs cap layer, doped $Al_xGa_{1-x}As$ layer, thin undoped $Al_xGa_{1-x}As$ spacer layer, thick undoped GaAs buffer layer, and semi-insulating GaAs substrate. A two-dimensional free-electron gas is formed at the interface between the undoped $Al_xGa_{1-x}As$ and GaAs buffer layers, separated by the spacer layer from the nearest donors in $Al_xGa_{1-x}As$ layer. A typical device, the so-called high-electron-mobility transistor, has a metal gate with a conductive channel width much larger than the distance between source and drain ($>10:1$). Other samples employ a van der Pauw (VDP) square geometry with an ohmic contact in each corner.

Samples from two different sources were used. Summarized in Table I are their principal parameters: the

TABLE I. Principal parameters of samples. Sample label, cap-layer thickness L_c, cap-layer doping density $N_{d,c}$, $Al_xGa_{1-x}As$ layer thickness L_a, $Al_xGa_{1-x}As$ layer doping density $N_{d,a}$, undoped spacer thickness L_s, gate voltage threshold (V_t) at 77 K in the dark, the net ionized donor density N_i in depleted $Al_xGa_{1-x}As$ layer at 77 K in the dark, and the percentage increase of N_i after identical brief white light illumination sufficient to saturate the PPC change. Layer thicknesses are in units of nm and doping/carrier densities are in units of 10^{17} cm^{-3}. All samples had an aluminim fraction $x=0.3$ in the doped $Al_xGa_{1-x}As$ layer.

Sample	L_c	$N_{d,c}$	L_a	$N_{d,a}$	L_s	V_t	N_i	$\Delta N_i/N_i$
B[a]	50	2	100	10	5	−0.5 V	1.9	15%
C[b],D[b]	20	10	30	10	10		ungated VDP	

[a]Tek: Tektronix Inc., R. Gleason and R. Koyama.
[b]Cornell: Cornell University, W. Schaff.

cap-layer thickness L_c, cap-layer doping density $N_{d,c}$, $Al_xGa_{1-x}As$ layer thickness L_a, $Al_xGa_{1-x}As$ layer doping density $N_{d,a}$, and undoped spacer thickness L_s. Table I includes the threshold gate voltage (V_t), and net ionized donor density N_i in the depleted $Al_xGa_{1-x}As$ layer at 77 K in the dark, as well as the percentage increase of N_i after saturated PPC for sample B. Sample D, an ungated VDP square, had $x=0.3$ in the Si-doped $Al_xGa_{1-x}As$ layer but $x=1.0$ in the undoped spacer layer and a 10 nm undoped $Al_xGa_{1-x}As$ layer ($x=0.3$) between the cap layer and the doped $Al_xGa_{1-x}As$ layer. Sample C has layer parameters similar to sample D but a different annealing temperature. For samples C and D (with relatively thin doped $Al_xGa_{1-x}As$ layers, $L_a=30$ nm) the in-dark band bending is like that shown in Fig. 1 and there are few free electrons in the $Al_xGa_{1-x}As$ layer. Table II shows the in-dark and following-light exposure carrier density and mobility of samples C and D at 77 K.

For sample B (a gated HEMT), the source-drain current I_{SD} was measured with a fixed source-drain voltage. For the ungated van der Pauw samples C and D, the carrier densities N_s were measured via the Hall effect. For example, [Fig. 3(a)] after illumination is removed, N_s of sample C decays with an initially fast decay, followed by a continuously decreasing decay rate. The decay is nearly a straight line when plotted as a function of $\log_{10}(t)$ for close to seven orders of magnitude in time indicating a wide range of the decay time constant [Fig. 3(b)]. Similar decay measurements of I_{SD} from sample B show this nonexponential result.

IV. ANALYSIS USING ln(t)-DERIVATIVE METHOD

In view of the possible decay mechanisms previously described detailed information about capture energies and lifetime prefactors is needed to distinguish among the different processes that contribute to TPC. In the following, we demonstrate how the temperature-dependent decay time can be analyzed using a ln(t) derivative technique (full details are found in Ref. 13). This yields a trap spectroscopy with characteristic energies and lifetime prefactors that differ so significantly for different capture mechanisms that phonon-assisted tunneling and other decay channels may be unambigously identified.

Assume a general form of multirate decay of the free-electron number density $N(t)$ at a fixed temperature T:

$$N(t)=\sum_i N_{i0}\exp(-t/\tau_i) , \tag{5}$$

TABLE II. This table presents the carrier densities and mobilites of van der Pauw samples C and D before and after light exposure at 77 K.

Sample	$N_s(10^{11}$ cm$^{-2})$	Mobility [cm^2/(V s)]
C	3.9 (dark)	65 000 (dark)
	4.97 (after light)	76 000 (after light)
D	3.67 (dark)	39 000 (dark)
	4.47 (after light)	46 000 (atfer light)

where N_{i0} is the initial number density of decay channel i, and with a corresponding individual lifetime τ_i.

Define a quantity $K(t)$, as the ln(t) derivative of $N(t)$, by

$$\begin{aligned} K(t) &= -dN/d[\ln(t)] \\ &= -t\,dN/dt \\ &= \sum_i (t/\tau_i)N_{i0}\exp(-t/\tau_i) . \end{aligned} \tag{6}$$

Notice in Fig. 4 that one decay channel produces a single peak in $K(t)$ (dot-dashed curve) with a width extending over a decade of time. A set of nonvanishing decay features extending over many decades in time indicates a band of decay channels whose characteristic energies and prefactors may be determined by tracking them over a range of T.

Consider the decay process over a narrow enough temperature range T to T' so only one decay mechanism dominates, and one can obtain the following relation between τ_i' and τ_i:

$$\tau_i' = \tau_i \exp[(E/kT') - (E/kT)] , \tag{7}$$

where E is the capture energy, and τ_i' is the new lifetime at T'. Assuming

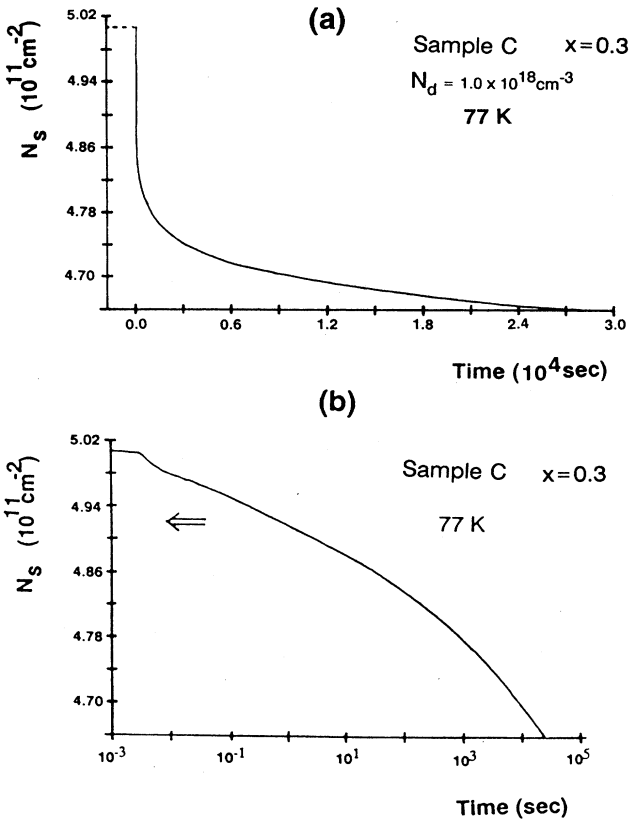

FIG. 3. Multiple-rate TPC decay in the carrier density, N_s from sample C at 77 K. (a) N_s plotted against t. (b) N_s plotted against log(t).

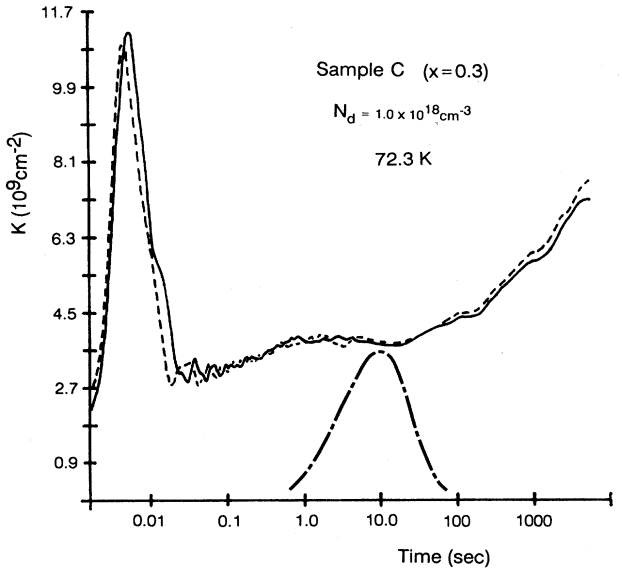

FIG. 4. $K(t)$ of sample C for repeated measurements at 72 K. For comparison, the dot-dashed curve is $K(t)$ for an arbitrary *single* rate decay with $\tau=10$ sec.

$$N'(t)=\sum_i N_{i0}\exp(-t/\tau_i') \tag{8}$$

is the form of the decay at T', the corresponding new value of $K(t)$ at T' is

$$K'(t)=\sum_i (t/\tau_i')N_{i0}\exp(-t/\tau_i') \ . \tag{9}$$

A plot of $K'(t)$ versus $\ln(t)$ will simply be displaced by $[(E/kT')-(E/kT)]$ from $K(t)$ at the same $\ln(t)$. Therefore, the capture energy E_c and the decay time prefactor can be determined from the temperature-dependent displacements of $K(t)$.

When the lifetimes for direct capture into one type of ionized donor and tunneling-assisted capture into another kind of donor are comparable within the same time window, the resulting mixture depends on the amplitude of each decay channel. The fewer the free carriers in the doped $Al_xGa_{1-x}As$ layer after type-A tunneling, the more difficult it is to distinguish a direct capture peak in $K(t)$ from tunneling-assited capture. However the temperature-induced shifts of different peaks or structures will vary if they have different thermal activations.

Although direct capture by DX centers in not very thick doped $Al_xGa_{1-x}As$ layers is difficult to detect, type-B tunneling-assisted capture by DX centers can easily be observed at high temperatures because this directly reduces the 2D electrons. So from Eq. (4), the DX-center capture energy can be deduced indirectly.

V. DETECTION OF PHONON-ASSISTED TUNNELING

This section presents the photodecay data from different samples and identifies the TPC mechanisms discussed in Sec. I. The TPC mechanisms are determined by analyzing the capture energies and lifetime prefactors over different temperature ranges.[14] Raising T speeds up each decay, but for a small enough temperature change, individual peaks or structure can be tracked. The characteristic activation energies of particular decay structures are obtained from their temperature-induced shifts in time.

$K(t)$ was determined from the decay of N_s for van der Pauw samples C and D and the decay of I_{SD} for HEMT sample B. In repeated measurements following illumination (sufficient to saturate I_{SD} or N_s), the $K(t)$ versus $\log_{10}(t)$ plot of the decay curve shows no significant shift of principal features at the same temperature. Data in Fig. 4 shows decay curves, repeated one after another for sample C with identical illumination before each decay. The main features of the data are also reproducible with different histories, such as random thermal cycling or previous illumination at different temperatures.

A. Sample C

Figure 5 shows the temperature dependence of $K(t)$ from sample C for 68 K $< T <$ 85 K. The sample was exposed to 1 sec of white light before each decay. The broad individual decay peaks can easily be tracked on top

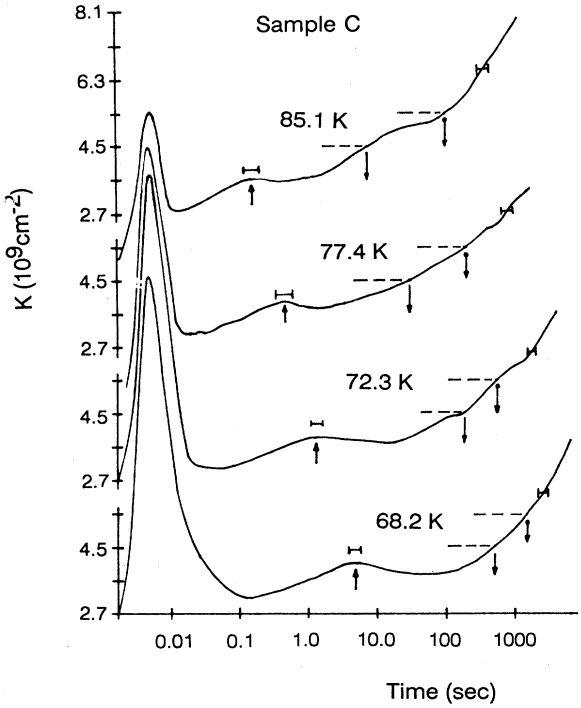

FIG. 5. $K(t)$ for sample C between 68 K $< T <$ 85 K. Up arrows indicate the positions of peaks near $t=1$ sec. Down arrows indicate the positions for specific values of $K(t)$ at each temperature. The horizontal error bars in this and the following figures indicate variations of the positions of either peaks or chosen values of $K(t)$ obtained from different TPC-decay measurements.

of a slowly increasing base line. The error bars indicate the variation for TPC decays repeated at the same temperature. Notice that the peak values of $K(t)$ (near 1 sec) are nearly the same when they shift with temperature. E_c' and τ_0 are deduced from the temperature dependence of the peak shifts. The peaks near 0.01 sec show nearly zero activation energy and $\tau_0 \sim 10^{-2}$ sec. This is identified as direct capture by shallow donors. But the capture energy obtained from peaks near 1 sec is 100 meV with $\tau_0 \sim 10^{-7}$ sec (which is much longer than the *DX*-center direct-capture prefactor of 10^{-11} sec). For longer times, there are no obvious peaks to track, but a slowly increasing structure is clear, corresponding to a band of decay channels whose overall horizontal shift for the *same* values of $K(t)$ can be tracked at different temperatures. The capture energy of tracks shown in Fig. 5 are measured to be 100 meV±20 meV with $\tau_0 \sim 10^{-3}-10^{-7}$ sec. The resulting high thermal activation energy (100 meV) and long-lifetime prefactors are consistent with the prediction in Fig. 2 for type-*B* tunneling-assisted capture (with a *DX* capture energy of 80 meV for $T=77$ K).

For higher temperature TPC decay in sample *C* (86 K $< T <$ 178 K, Fig. 6), the time window is set from 1 msec to 500 sec. In this temperature range, every curve shows a single decay peak (with a few msecs lifetime) that is followed by a slowly increasing baseline. The temperature dependence of the single fast-decay lifetime displays the bahavior of shallow donors seen at lower T (Fig. 5). For 160 $K < T <$ 178 K, a group of peaks are tracked that result in $E_c' = 340 \pm 40$ meV and $\tau_0 \sim 10^{-9}$ sec. This is interpreted as type-*B* tunneling-assisted capture, with a *DX*-center capture energy $E_c = 170 \pm 40$ meV, that is consistent with results from other work.[15,16]

B. Sample *D*

Figure 7 shows the shifts of decay groups with temperature on sample *D*. The broad individual decay peaks can be easily tracked on top of a slowly increasing base line for 130 K $< T <$ 145 K. Notice also that the peak values of $K(t)$ are nearly the same when they shift with temperature. The peak value of $K(t)$ is $\approx 1 \times 10^{10}$ cm^{-2}, which corresponds to a decrease in N_s of 1.2×10^{10} cm^{-2}. E_c' is measured to be 400±40 meV with $\tau_0 \sim 10^{-13}$ sec. This high apparent capture energy for 130 K $< T <$ 145 K is interpreted as type-*B* tunneling-assisted capture, and the resulting value of E_c is 230±40 meV, which is slightly higher than the results from samples *C* and *L* with the same Al fraction.

By contrast, in Fig. 8 (sample *D*) for 82 K $< T <$ 110 K, there are no obvious peak shifts to track, but a slowly increasing base-line structure becomes clear, whose overall horizontal shift at the same values of $K(t)$ can be tracked as a function of temperature. In addition note for comparision the superposition (dashed line) of the resulting $K(t)$ peak for a theoretical single rate decay process with $\tau_0 \sim 100$ sec. The capture energy of the experimental tracks is measured to be about 20 meV with $\tau_0 \sim 1-100$ sec. This lower activation energy and long-lifetime prefactor together with an increasing base-line structure is not explained by the results shown in Fig. 2.

The behavior of $K(t)$ for sample *D* was verified in an alternative decay experiment. A continuous temperature sweep at a constant rate of about 0.1 K/sec after il-

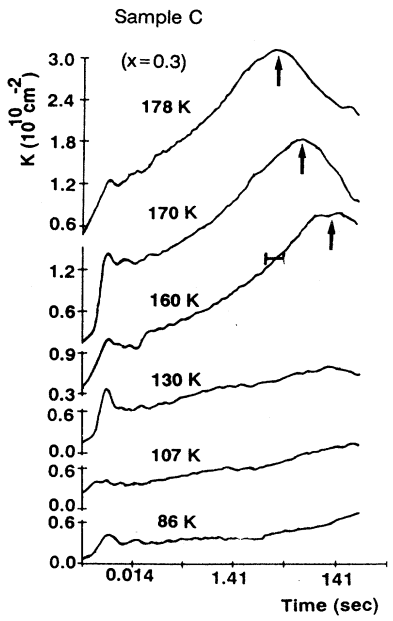

FIG. 6. $K(t)$ from sample *C* for 86 K $< T <$ 178 K. A 5 sec LED light pulse is used for illumination, with the data showing no significant change from exposure to white light.

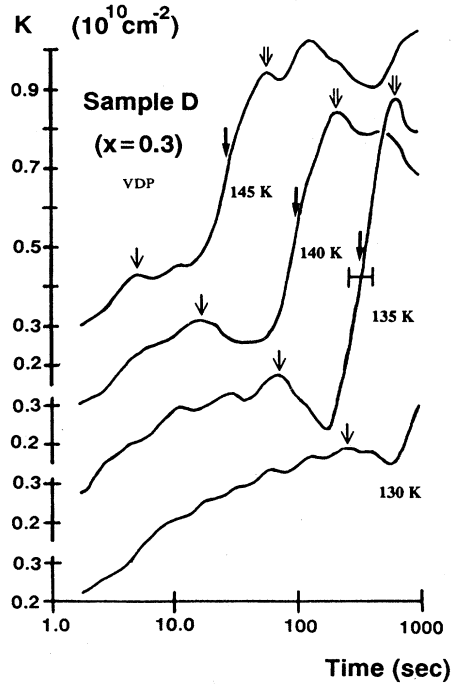

FIG. 7. $K(t)$ of sample *D* for 130 K $< T <$ 145 K. Tracked peaks are indicated by short arrows and the "shoulders" are indicated by long arrows.

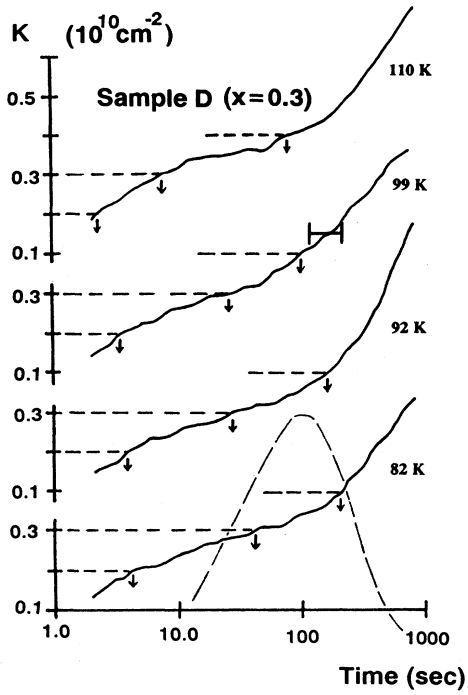

FIG. 8. $K(t)$ of sample D for 82 K $< T <$ 110 K. In comparison, the dashed curve is $K(t)$ for a single rate decay with $\tau = 100$ sec. Down arrows indicate the time positions for chosen values of $K(t)$.

lumination is shown in Fig. 9. When the sample is warmed from 77 K, a sudden dip in carrier density is observed (see arrow) when T passes through 150 K, which agrees with the temperatures where large-$K(t)$ peaks were observed in Fig. 7. The decrease in N_s ($\approx 1.5\times10^{10}$ cm^{-2}) is in good agreement with the value (1.2×10^{10} cm^{-2}) obtained from the peak value of $K(t)$ in Fig. 7.

C. Sample *B*

Figure 10 is an example of TPC decay in sample B (from conductivity measurements) from 55 K $< T <$ 74 K. $K(t)$ displays a monotonically increasing base-line structure and has almost zero thermal activation energy. The monotonic behavior of $K(t)$ indicates that the decay is occurring from a range of decay channels over a continuous spread of relaxation rates. At zero gate voltage (V_g), there are some free electrons from shallow donors ($\sim$20% of the total donors for the case of $x = 0.3$) in the thick (100 nm, much wider than W_d in-dark) doped $Al_xGa_{1-x}As$ layer. E_{CB} will line up with E_0 of the 2D EG (unlike the case shown in Fig. 1), so that no type-B tunneling-assisted decay takes place. After type-A tunneling, thermally activated behavior by direct capture to deep centers over a narrow intermediate temperature range 60 K $< T <$ 80 K was expected, considering the results of other work on bulk material[17] and by decay of the threshold voltage which is sensitive to direct capture to deep centers in the $Al_xGa_{1-x}As$ layer.[15] However the results of this work show that the carrier density in the $Al_xGa_{1-x}As$ layer was not sufficient to produce a signal from direct capture that was large enough to be clearly detected from the decay background.

Figure 11 shows $K(t)$ from sample B for 122 K $< T <$ 159 K ($V_g = 0$) resulting in $E_c = 170\pm20$ meV and $\tau_0 \sim 10^{-6}$ sec. This energy is too low to agree with the apparent capture energy ($E_c' = 340$ meV) of type-B tunneling-assisted decay in the same temperature range. This is consistent with the fact that type-B tunneling-assisted capture is not expected in this case where in a

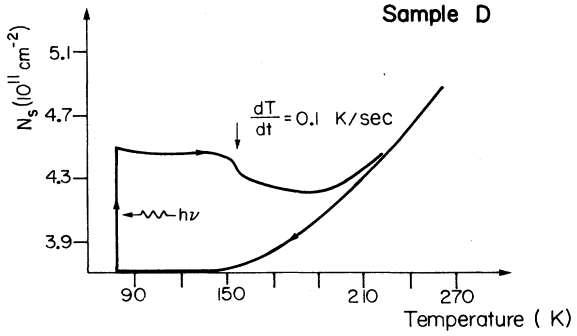

FIG. 9. Temperature-sweep method of observing elevated TPC decay at special temperatures (arrow) for sample D.

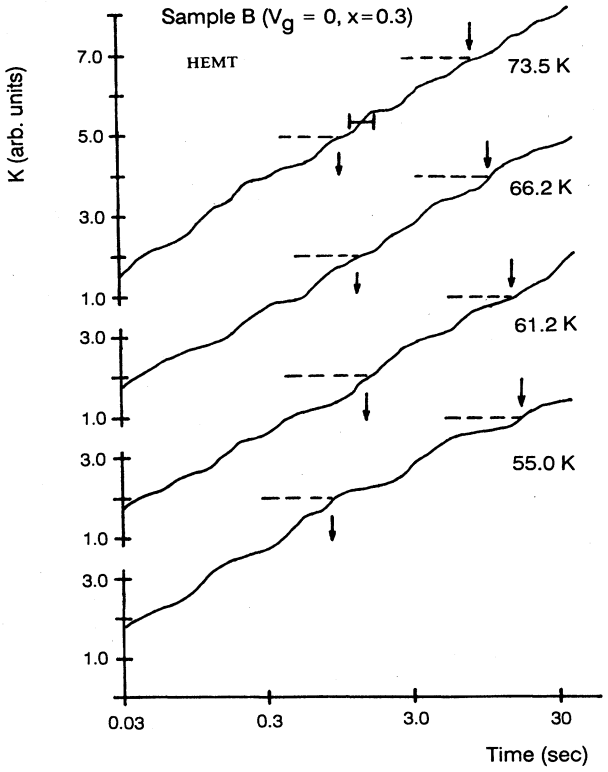

FIG. 10. $K(t)$ of HEMT sample B for 55 K $< T <$ 74 K ($V_g = 0$). Down arrows indicate the time positions for chosen values of $K(t)$.

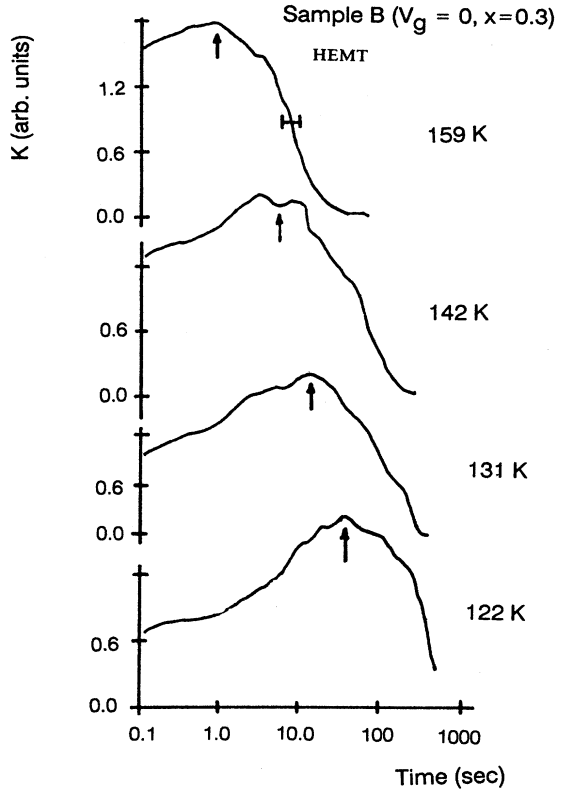

FIG. 11. $K(t)$ of HEMT sample B for 122 K $< T <$ 159 K ($V_g = 0$).

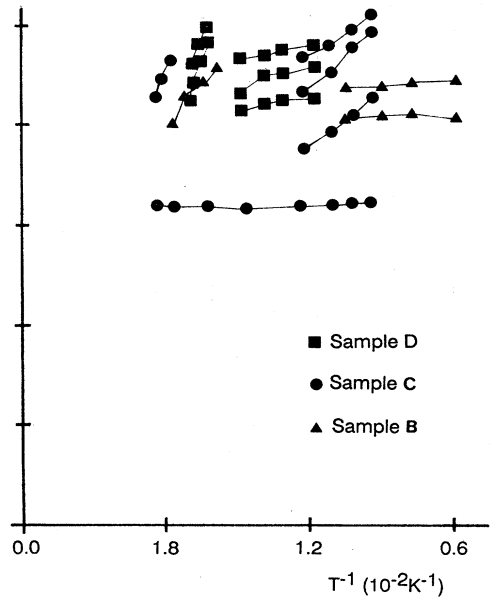

FIG. 12. Summary of the tracked peaks or other $K(t)$ structures. The lines for sample D (82 K $< T <$ 110 K) and HEMT sample B (55 K $< T <$ 74 K), and the upper two lines from sample C (68 K $< T <$ 85 K) are obtained from the horizontal shifts of chosen values of $K(t)$. Data connected by solid lines are consistent with the picture represented in Fig. 2, whereas data connected by dashed lines are not.

thick doped $Al_xGa_{1-x}As$ layer (100 nm) E_{CB} does not rise above E_0.

VI. SUMMARY

Using an analysis method based on $dN/d[\ln(t)]$ (or alternatively $dI_{SD}/d[\ln(t)]$) we have been above to detect distinct decay features of transient photoconductivity in $GaAs/Al_xGa_{1-x}As$ heterostructures. This method was employed on different heterostructures and HEMT devices. The results permitted us to identify the contribution to TPC of phonon-assisted tunneling from other PPC-decay mechanisms.

The thermal activation features described in the previous section are summarized in Fig. 12. The results, which are consistent with the predictions in Fig. 2, are connected by solid lines. The data shows TPC decay occuring mainly through direct capture by shallow traps and type-B tunneling-assisted capture by deep traps in the $Al_xGa_{1-x}As$ layer. At temperatures near 77 K, only deep-trap-related type-B tunneling-assisted decay (with $E_c = 80 \pm 20$ meV) was observed within the time window 10^{-3}–10^4 sec. At temperatures near 160 K, trap-related type-B tunneling-assisted decay dominates (with capture energy between 170–230 meV).

The DX-center capture energies ($E_c = 80$–230 meV) for $x = 0.3$ deduced from type-B tunneling-assisted decay are in reasonable agreement with results ($E_c = 110$–200 meV) from other work.[14,15] Direct capture by deep traps in the $Al_xGa_{1-x}As$ layer was not observed due to the low mobility and small number of free electrons in this layer, hence their relatively small contribution to the transport current compared to that of the 2D EG.

Other data connected by dashed lines are not consistent with the picture in Fig. 2. For example, low activation energy ($E_c < 20$ meV) features are present for 50 K $< T <$ 110 K but with lifetime prefactors longer ($\tau_0 > 1$ sec) than the tunneling calculation of Fig. 2 would permit. Also, thermally activated behavior with $E_c = 170$ meV and $\tau_0 \sim 10^{-6}$ sec is present for 120 K $< T <$ 160 K in HEMT sample B ($V_g = 0$). This capture energy is too small to agree with type-B tunneling-assisted decay at the same temperatures. All of the above long prefactors indicate the involvement of tunneling-assisted decay. These features are consistent with the experimental results[3] which led to the proposal of 2D-electron virtual-state impurity tunneling. Since the proposed virtual states are not yet clarified, more theoretical modeling and experimental work are needed to determine its contribution to TPC.

ACKNOWLEDGMENTS

This work was supported by the NSF-DMR Grant Nos. 81-19550, 81-13456, and 85-19728 and by the Tektronix Foundation. It is a pleasure to thank K. R. Gleason (Tektronix) and W. Schaff (Cornell) for supply-

ing useful samples and J. D. Cohen and J. C. Overley (University of Oregon) for helpful discussions.

APPENDIX

Expressions for the tunneling barrier $U(z)$, which begins from the level $E_{\rm th}$ above E_0, and the tunneling barrier width z_0 are calculated as follows for conduction-band bending [shown as the solid cruve in Fig. 1(a)] after illumination. $U(z)$ and z_0 are determined from $E_{\rm th}$, ΔE_c, and L as shown in Fig. 1(a), and the ionized donor number density N_i (in units of 10^{18} cm^{-3}). All energies are in units of eV, and all distances are in nm.

The value of the depletion width after type-A tunneling ($W_d=z_1-L$) is obtained by

$$\Delta E_c-E_0=[(z_1-L)^2+2L(z_1-L)]N_i/1458 . \quad \text{(A1)}$$

Given a value of the depletion width ($W_d=z_2-L$) at this moment with band bending shown as the solid curve in Fig. 1(a), the difference between the $Al_xGa_{1-x}As$ layer conduction-band minima and E_0 of 2D EG is

$$\Delta E=[(z_2-L)^2+2L(z_2-L)]N_i/1458-\Delta E_c+E_0 , \quad \text{(A2)}$$

and the value of U_0 shown in Fig. 1(a) is

$$U_0=(z_2-L)^2N_i/1458 . \quad \text{(A3)}$$

Then, in the case of $U_0-\Delta E>E_{\rm th}$, i.e., $z_0>L$, we have

$$z_0=z_2-[(\Delta E+E_{\rm th})1458/N_i]^{1/2} . \quad \text{(A4)}$$

There are two formulas for $U(z)$. If $z<L$,

$$U(z)=(\Delta E_c-E_0-U_0+\Delta E)(1-z/L)+U_0-\Delta E-E_{\rm th} ; \quad \text{(A5)}$$

but if $z>L$,

$$U(z)=U_0[1-(z-L)/(z_2-L)]^{1/2}-\Delta E-E_{\rm th} . \quad \text{(A6)}$$

In the case of $U_0-\Delta E<E_{\rm th}$, i.e., $z_0<L$, there are different formulas:

$$z_0=L(\Delta E_c-E_0-E_{\rm th})(\Delta E_c-E_0-U_0+\Delta E)^{-1} \quad \text{(A7)}$$

and

$$U(z)=(\Delta E_c-E_0-U_0+\Delta E)(1-z/L)+U_0-\Delta E-E_{\rm th} . \quad \text{(A8)}$$

The above equations can be applied to type-B tunneling by replacing z_2 and U_0 by their counterparts z_2^* and U_0^* [Fig. 1(b)].

---

*Corresponding author.

[1]For a recent review see M. I. Nathan, Solid-State Electron. **29**, 167 (1986).

[2]D. E. Theodorou and H. J. Queisser, J. Appl. Phys. **23**, 121 (1980).

[3]E. F. Schubert, A. Fischer, and K. Plogg, Phys. Rev. B **31**, 7937 (1985).

[4]D. V. Lang and R. A. Logan, Phys. Rev. Lett. **39**, 635 (1977).

[5]D. V. Lang and R. A. Logan, Phys. Rev. B **19**, 1015 (1979).

[6]K. L. I. Kobayashi, Y. Uchida, and H. Nakashima, Jpn. J. Appl. Phys. **24**, L928 (1985).

[7]H. J. Queisser and D. E. Theodorou, Phys. Rev. **33**, 4027 (1986).

[8]E. F. Schubert and K. Ploog, Phys. Rev. **29**, 4562 (1984).

[9]E. F. Schubert, J. Knecht, and K. Ploog, J. Phys. C **18**, L215 (1985).

[10]N. Chand, T. Henderson, J. Klem, W. T. Masselink, R. Fischer, and H. Morkoç, Phys. Rev. B **30**, 4481 (1984).

[11]The pure-tunneling lifetime can be estimated as $Wv^{-1}p^{-1}$, where W is the width of the potential well at the 2D interface, v is the z-direction velocity of the 2D electrons deduced from the z-quantized ground-state energy E_0 plus a thermal energy in the case of phonon-assisted tunneling. Using as estimate of $W\sim10^{-6}$ cm, and $v\sim10^8$ cm sec^{-1} along with the range of pure-tunneling probabilities (10^{-6}–10^{-10}) from the WKB integral, one gets tunneling lifetimes between 10^{-8} to 10^{-4} sec.

[12]O. Madelung, *Introduction to Solid-State Theory* (Springer, New York, 1978), p. 177.

[13]L. X. He, K. P. Martin, and R. J. Higgins, Phys. Rev. B **36**, 6508 (1987).

[14]For convenience, the value of $K(t)$ obtained from this data is with respect to $\log_{10}(t)$, which is a factor of 2.30 different than the value defined by Eq. (6). In this way, a single-rate decay with an amplitude of N_{00} corresponds to an experimental result of $K(t)$ with a peak value of $0.85N_{00}$.

[15]P. M. Mooney, Bull. Am. Phys. Soc. **32**, 504 (1987).

[16]P. M. Mooney, N. S. Caswell, P. M. Solomon, and S. L. Wright, Mater. Res. Soc. Symp. Proc. **46**, 403 (1985).

[17]R. J. Nelson, Appl. Phys. Lett. **31**, 351 (1977).